

Supporting information

Antifolate SERS-active nanovectors: quantitative drug nanostructuring and selective cell targeting for effective theranostics

C. Fasolato*, S. Giantulli, A. Capocéfalo, Y. Toumia, D. Notariello, F. Mazzarda, I. Silvestri, P. Postorino, F. Domenici*

*corresponding authors

C.Fasolato: claudia.fasolato@unipg.it

F.Domenici: fabio.domenici@uniroma2.it

SI 1 - Preparation protocol

The synthesis of the nanovector is described as follows:

1. Gold nanoparticles (NPs) are functionalized with the Raman reporter **4-aminothiophenol (4ATP)**. The used NPs are 60 nm sized gold nanocolloids stabilized by citrate capping in water dispersion and were purchased by Ted Pella. The functionalization process consists in adding a small volume fraction of 4ATP in ethanol solution to the NP dispersion, so that the final 4ATP concentration (0.1 mg/mL) exceeds the amount of 4ATP necessary for the complete coverage of the NP surface, as estimated by steric hindrance arguments [**Fas2014**];
2. the sample of 4ATP-NP was then purified with a 12- to 24-hour long **dialysis** against ultrapure (milliQ) water;
3. **activation of folate and antifolate** functional groups by the subsequent use of EDC(1-ethyl-3-[3-dimethylaminopropyl] carbodiimidehydrochloride) and NHS (N-hydroxy-succinimide), necessary for the binding of these molecules to the 4ATP-AuNP system;
4. **incubation** of 4ATP-NPs with the activated folate/antifolate, for 12 hours at 4°C, to induce the covalent binding of the two species;
5. after the final step of the bioconjugation, the sample was further purified by a 24 hours **dialysis** against milliQ water; this final step allows to control the final size of the colloid by eliminating the folate corona that might arise around the biofunctionalized NPs.

The preparation and purification protocols adopted for obtaining our folate/antifolate nanovectors were carefully optimized by several characterization techniques, among which AFM imaging: The produced nanovector dispersions were deposited on coverslip glass slides and the NP adhesion to the substrate was obtained by drying the sample under controlled environmental conditions, as described in [**Fas2014**].

In **Figure S1**, we compare the AFM images acquired on two substrates obtained by different sample batches of folic acid (FA) functionalized nanovectors, FA-NVs. In the case presented in panel A, the dialysis time was too short (6 hours) and indeed a sort of halo is visible around the NPs. This suggests the presence of an excess of physisorbed folate molecules around the NPs. Indeed, the effect is not visible on samples in which the dialysis lasted for longer times. that is eliminated by a longer (24 hours) dialysis time.

A Dimension Icon microscope equipped with a Nanoscope V Controller (Bruker AXS, Germany) in tapping mode was used for AFM images. High resolution probes with extremely sharp tip (nominal radius of curvature of 2 nm) were employed.

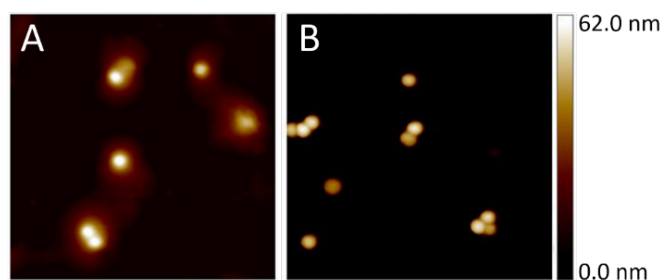


Figure S1: AFM images acquired on FA-4APT-NP assemblies on coverslip glass slides. The image side in A corresponds to a 1.3 μm scale, while in B to a 1.5 μm scale. The residual folate corona revealed in A is not detected when the purification time is optimized, as in B.

SI 2.1 - Successful functionalization: UV-Visible

We can prove the successful functionalization of the realized samples by different methods, among which UV-Visible absorption spectroscopy is one of the most powerful. As discussed in detail in the main text (Figure 2A and discussion), the most immediate proof of the conjugation comes from the redshift of the plasmonic peak that takes place in going from the bare gold NPs, to the conjugated 4ATP-NPs, and is even more pronounced in the case of FA-4ATP-NPs.

Another possibility is to measure the molecular electronic excitation ascribed to the presence of folate/antifolate and 4ATP in solution. An example is displayed in **Figure S2**, where we compare the UV-Visible absorption spectrum of the bare AuNP dispersion with the one obtained at the two other steps of the functionalization: 4ATP-NPs (step 1. of the preparation discussed in SI 1) and FA-4ATP-NPs (step 3. of the preparation discussed in SI 1). In the case of 4ATP-NPs, we observe at short wavelengths (250 nm) the electronic absorption bands of molecular 4ATP, which are very pronounced because the sample has not yet been purified. Similarly, in the case of FA-4ATP-NPs, we reveal the electronic absorption bands of FA around 280 nm. AMT and MTX feature analogous absorption profiles.

It is worth mentioning that the UV absorption bands of the molecule, when the sample is purified, are much weaker than the ones revealed in the spectra of **Figure S2**. Indeed, the overall concentration of 4ATP and folate/antifolate molecules in the purified samples results fairly below the micromolar range. This is also why, in the spectrum of the FA-NV (red in **Figure S2**), the bands of 4ATP are not as strong as the ones detected on the 4ATP-NP conjugate (blue spectrum in **Figure S2**).

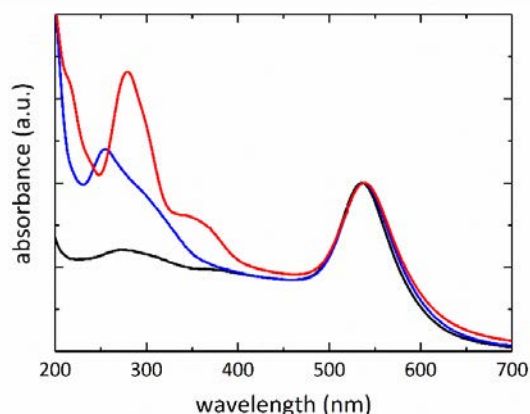


Figure S2: UV-Visible absorption spectra acquired at three steps of functionalization: bare plasmonic NPs (black), 4ATP-NPs (blue), FA-4ATP-NPs (red). The spectra are normalized to the absorption of the plasmonic NPs.

SI 2.1.1 – Comparison of UV-Visible plasmonic peak shift with titration results

In Figure 2 of the main text, the results of two generally accepted titration methods, along with the SERS titration approach here proposed, are presented. In panel A, UV-Visible absorption spectra show a shift of the plasmonic peak upon functionalization of the NPs. This is clearly visible in going from the bare, citrate capped AuNPs ($\lambda_{NPS} = 535.0 \pm 0.5$ nm as estimated by the first derivative of the spectrum) to 4ATP-NPs ($\lambda_{4ATP} = 535.0 \pm 0.5$ nm), to the complete systems, namely FA-NVs ($\lambda_{FA} = 538.5 \pm 0.5$ nm), MTX-NVs ($\lambda_{MTX} = 538.0 \pm 0.5$ nm) and AMT-NVs ($\lambda_{AMT} = 540.0 \pm 0.5$ nm). The spectral shift is ascribed to the change in the dielectric environment of the NP occurring upon functionalization, first with 4ATP, then with the drug molecules. In principle, the shift is expected to be proportional to the effective dielectric constant of the medium surrounding the NP, which is composed of 4ATP ligand molecules, drug molecules, and water. The higher the number of molecules bound to the NP, the higher the effective refractive index of the surrounding medium, the more pronounced the redshift of the plasmonic peak one can reasonably expect.

In panel B of Figure 2, we present the results on the AMT-NV of a standard colorimetric titration test based on a fluorescent dye (Orange II). The procedure adopted for these standard measurements is described in the Experimental Section. Data similar to the ones of Figure 2B are available for all the three types of NV. Indeed, the number of drug molecules bound to the NPs, as extrapolated from the titration measurements, were used as x-axis data for producing panel 2D.

In the following **Figure S3**, which we added to the Supporting information, the trends of the UV-Visible plasmonic absorption peak and of the colorimetric titration data are compared. A clear agreement between the two measurements is visible. However, extracting a quantitative estimate of the number of molecules from UV-Visible spectra of this sort is quite difficult, considering that

- (i) the plasmonic peak is a broad spectral feature, and we here monitor frequency shifts that are about the 2% of the peak width;
- (ii) the redshift of the plasmonic peak can be ascribed not only to the change in the dielectric environment, but also on other phenomena, as the accidental occurrence of NP aggregation within the NV dispersion.

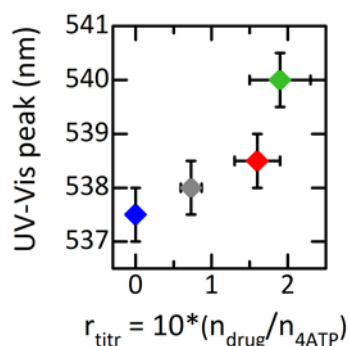


Figure S3: UV visible peak central wavelength (nm) is compared to the colorimetric titration ratio, calculated as described in the main text.

SI 2.2 - Successful functionalization: Dynamic Light Scattering and ζ Potential

We can monitor the size of the obtained nanocolloids by means of Dynamic Light Scattering (DLS) measurements, as shown in **Figure S4**. We notice that the biofunctionalization increases the size of the NPs from $d \sim 67$ nm to $d \sim 74$ nm in the FA and AMT cases, while the revealed NV size is slightly bigger ($d \sim 87$ nm) in the case of the MTX-NV. This can be ascribed to a weak aggregation effect, probably due to the less dense, therefore less homogeneous, MTX molecular covering of the 4ATP-NPs. This observation is coherent with the data presented in Figure 2 of the main text, providing a clear experimental evidence of a less efficient MTX conjugation with respect to FA and AMT.

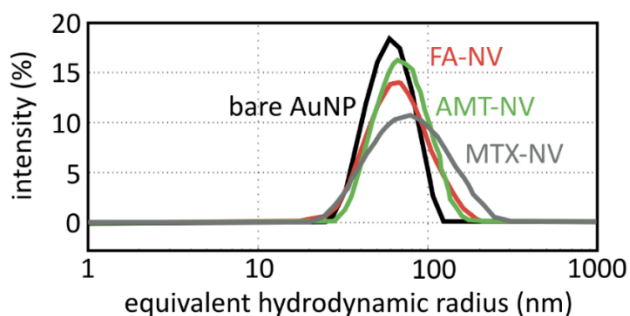


Figure S4: DLS size measurements on pristine gold NPs as purchased (black line, $d \sim 67$ nm) compared to the results obtained on the functionalized nanovectors: FA-NVs (red, $d \sim 73$ nm), AMT-NVs (green, $d \sim 74$ nm), MTX-NVs (gray, $d \sim 87$ nm).

The colloidal stability of the conjugated systems is a very important parameter for a nanosystem conceived for bioapplications and designed to be capable of traveling within very complex physiological media as cell culture medium, human serum or blood. In the present case, the DLS data suggest a good stability of the nanovector in solution, given the small NP size revealed (**Figure S4**). The result is further corroborated by ζ potential measurements, presented in **Figure S5**, that allow to assess the surface charge of our NV. The gold NPs, as purchased, are stabilized by citrate capping layer that is electrostatically bound to the NP surface and grants the stability of the nanocolloid. The citrate layer is removed by the covalent functionalization with 4ATP, which decreases the absolute value of the surface charge. The stability is restored ($|\zeta \text{ potential}| > 20$ mV) as the NPs are further conjugated with FA-, AMT- and MTX-. Indeed, as sketched in Figure 1 in the main text, in these systems the negative charge is provided by one of the two carboxyl groups of the folate/antifolate molecule.

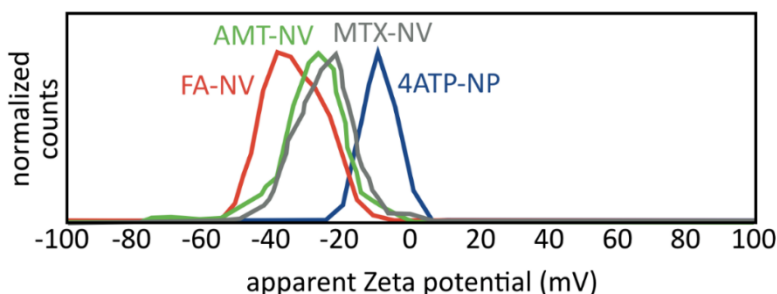


Figure S5: ζ potential measurements acquired on a suspension of 4ATP-NPs (blue line) compared to the results obtained on FA-NVs (red), AMT-NVs (green) and MTX-NVs (gray).

SI 3 – Infrared absorption

In **Figure S6**, we report the Fourier Transform Infrared Absorption spectra acquired on a deposition of AMT- and MTX-NVs performed by repeatedly dropcasting the NV dispersion on a CaF_2 window. Measurements were acquired in transmission, by integrating the signal over the whole substrate (10 mm diameter). The infrared signature of these

system, although a weak surface-enhanced infrared absorption effect takes place owing to the presence of the NP, is very modest, due to the small amount of molecules bound to the NP surface.

The most prominent spectral features are associated with the CC-stretching modes of the phenyl rings of both 4ATP and AMT/MTX, but the shoulder centered around 1700 cm^{-1} is assigned to the carbonyl group ($-\text{CONH}-$ in the case of antifolate-4ATP-NP).

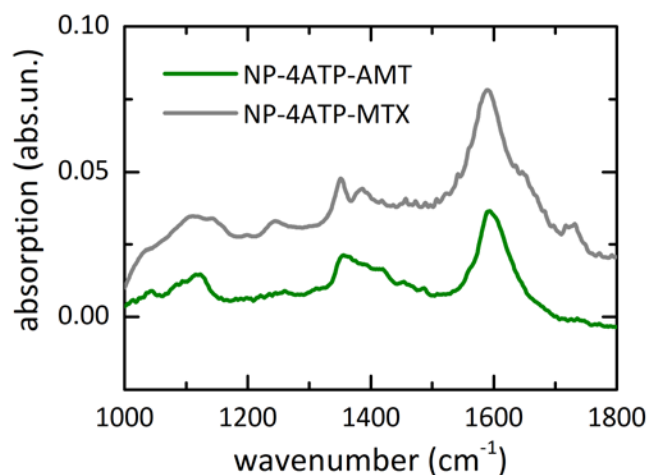


Figure S6: Infrared absorption spectra acquired on a dried deposition of the two antifolate nanovectors.

SI 4 - SERS spectra

SI 4.1 A more detailed discussion

The SERS data are worth a more detailed discussion. In **Figure S7**, in particular, we report the complete SERS spectra, acquired in the fingerprint region, for FA-, AMT-, and MTX-NVs, normalized to the most intense peak (CC stretching band around 1580 cm^{-1}). The spectra here presented are the mean of multiple acquisitions and are displayed after a linear background subtraction. We stress that we are presenting measurements performed by careful, high resolution mapping of micro-sized clusters obtained by self-assembly from the NV dispersion, thus we are sensitive to the effects induced by NP aggregation in terms of intensity and/or spectral shape. We have carefully set the measurement conditions and adjusted the adopted protocol so that we could obtain reproducible and reliable SERS spectra.

The procedure adopted to acquire the spectra is the one discussed in the Materials and Methods section of the main text. Here we used a 600 lines/mm diffraction grating, resulting in a final spectral resolution better than 3 cm^{-1} .

In all the spectra, the characteristic spectral features of the 4ATP SERS reporter are clearly recognizable [**Fas2014**, **Kim2011**]. Among these, the most intense are the well known C-S stretching band around 1078 cm^{-1} and the ring CC stretching band, already commented in the main text, around 1580 cm^{-1} . A certain variability of the spectral shape from sample to sample is observed, especially in correspondence of the spectral features marked by the dashed arrows in **Figure S7**. These bands are ascribed to b_2 symmetry vibrations of the 4ATP, and would in principle be forbidden by Raman selection rules. Their activation has to be ascribed to the “chemical enhancement”, that accounts for the changes in the molecular polarizability (and, therefore, for the relaxation of the Raman selection rules) related to the molecule proximity to the metal surface. A thorough discussion of the activation/deactivation of these bands in 4ATP

SERS spectra acquired on different metal substrates and/or in different conditions (e.g. different polarization of the substrate, different NP assembly conditions, occurrence of plasmon-induced molecular reactions etc.) is presented in references [Osa1994, Zho2006, Fas2018]. A tunable intensity of these bands was even reported by Moskovits and coworkers by tuning the interparticle distances in substrates obtained by self-assembly [Kim2011]. We believe that a slightly different NV assembly at the nanoscale is the reason why we observe such variability in our NV spectra.

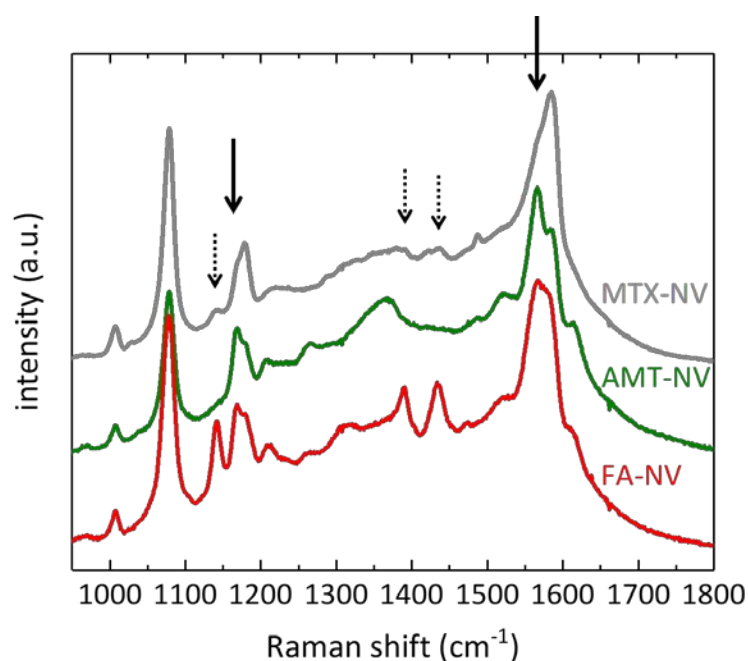


Figure S7: SERS spectra (fingerprint region) acquired on FA- (red), AMT- (green), MTX-NVs (gray line). Spectra are presented after a linear baseline subtraction and are vertically shifted for clarity. Solid black arrows marks the peaks that can be used as markers for folate/antifolate conjugation. The dashed arrows mark the b2 symmetry peaks that are variably enhanced and do not correlate directly with the titration ratio.

In our previous work, we highlighted that the most pronounced modification to the SERS spectra of 4ATP upon conjugation of FA was a change in the shape of the CC stretching band around 1580 cm^{-1} , reflecting a change in the relative weight of the two components (lower and higher frequency being ascribed to antisymmetric and symmetric CC stretching mode, respectively) [Fas2016]. In the present work, we point out that not only this spectral modification accounts for the occurrence of the conjugation with folate/antifolates, but also that this effect can be used to quantify the yield of the conjugation reaction, by comparison with other titration methods (see Figure 2 in the main text and related discussion).

A thorough analysis of the spectra in **Figure S7** reveals that another weak and yet reproducible spectral change is revealed upon conjugation, that is the appearance of a low frequency ($1168 \pm 1\text{ cm}^{-1}$) shoulder of the CH stretching band ($1180 \pm 1\text{ cm}^{-1}$). The two bands of interest are indicated by the solid arrows in **Figure S7**.

In **Figure S8**, we report the correlation between the ratio of the low and high frequency components of the bands of interest for SERS titration, at 1180 and 1580 cm^{-1} , and the result of the two-component fit in the representative case of MTX-4ATP-NPs.

The result of the analysis was found to be solidly reproducible on measurements from different sample batches and suggests that the activation of the low frequency components of these two bands is related to some charge redistribution occurring upon functionalization.

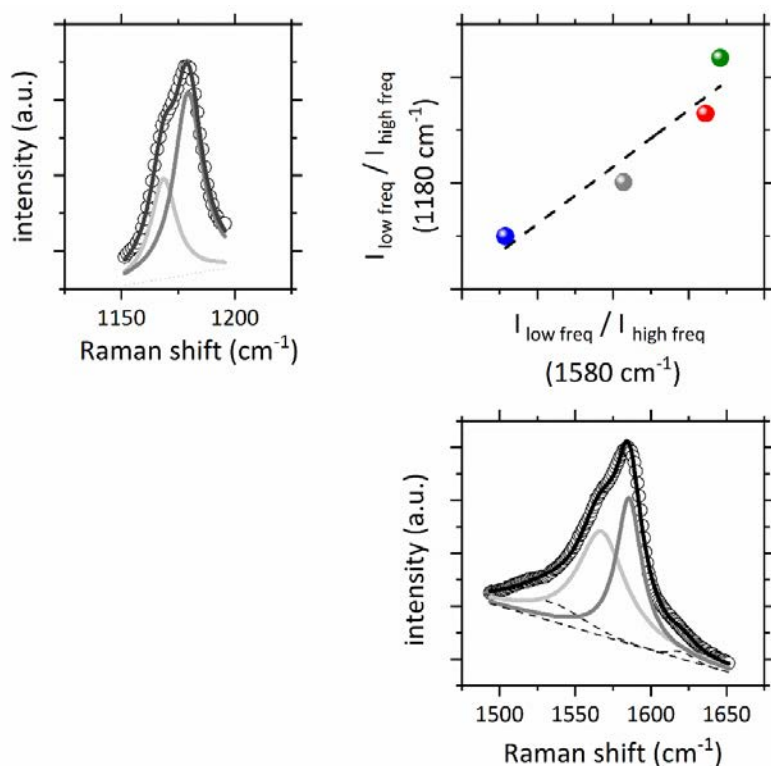


Figure S8: Top left panel, example of the fitting of the CH stretching band (1180 cm^{-1}) in the case of the MTX-NV. Bottom right panel, example of the fitting of the CC stretching band (1580 cm^{-1}) in the case of the MTX-NV. Central panel (up right), correlation between the SERS ratios for the two bands: the x,y values for the plot are calculated as the ratio between the low frequency component (light gray line in the spectra) and high frequency component (dark gray line in the spectra) of the bands at 1580 cm^{-1} and 1180 cm^{-1} , respectively.

SI 4.2: SERS frequency shift

The occurrence of a spectral weight redistribution in the SERS spectra of simple reporter molecules bound to plasmonic NPs is well accepted in the literature. It has been discussed early in 2012 by Kho and coworkers, also referenced in the main text [Kho2012]. This pivotal paper set the basis for a series of publications on SERS-immunoassays monitoring the frequency shift occurring in SERS spectra as a consequence of molecular binding events for the quantification of specific analytes, bound to the SERS reporter molecules on the NP surface (among the relevant works in the field, see for example references [Gue2013, Wan2014, Tan2016, Zhu2018] and references therein).

The characteristic spectral modifications observed in the papers listed above, and in similar works, have been ascribed to modifications induced to the SERS reporter by the analyte binding, either arising from the reorientation of the reporter molecule with respect to the NP surface, causing a change in the Raman selection rules, or from a deformation of the molecular structure and the consequent rearrangement of the molecular electronic cloud. The most common SERS reporters are usually small molecules, containing a phenyl group bound to various substituents, as in the case of 4ATP. Since these molecular systems are well studied, quite some literature is available for their specific Raman bands. The CC-stretching band at $\sim 1580\text{ cm}^{-1}$ we show in Figure 2 of the main text, indeed, is adopted as reference in numerous works (see e.g. references [Kho2012, Gue 2013] and citing papers).

In our previous work, we observed a shift in the central frequency of the 4ATP CC-stretching band around 1580 cm^{-1} arising upon functionalizing 4ATP-NPs with folate molecules. In ref. [Fas2016], we highlighted the effect by a Lorentzian fitting of the data, showing that the observed frequency shift derived from a change in the relative intensity of the two peaks composing the band. In the present work, we quantitatively correlate the observed change in the

spectral shape with the folate/antifolate ligand conjugation efficiency, as estimated by standard colorimetric titration tests.

Intuitively, since we ascribe the observed spectral shift to a change in the spectral weight of the two components (b- and a- symmetry modes, respectively), the most direct way to extract a quantitative estimate of this effect is to calculate the ratio between the intensities of the two components. which is why we have defined r_{SERS} as the ratio between the relative b- and a-symmetry peak intensities (ρ) in the conjugated and unconjugated (reference) cases. In the literature, the SERS spectral modification due to the molecular binding is quantitatively characterized either by calculating a nominal frequency shift derived by data fitting (e.g. [Kho2012, Zhu2018]) or by the calculation of the SERS spectral weight redistribution as antisymmetric to symmetric intensity ratio (e.g. [Gue2013]). The definition of r_{SERS} discussed in the main text is substantially a rescaling of the antisymmetric to symmetric intensity ratio ρ .

The r_{SERS} parameter and the CC-stretching band frequency shift follow the same trend as a function of the conjugated drug concentration. To prove so, one can calculate the frequency shift as $\Delta\nu = \langle\nu\rangle_{drug} - \langle\nu\rangle_{4ATP}$, being the reference frequency $\langle\nu\rangle_{4ATP}$ the one observed in the 4ATP-NP complex, and the frequency $\langle\nu\rangle_{drug}$ the one observed on FA-, AMT- or MTX-4ATP-NPs. The frequency of the band in the various cases can be defined as the first momentum of the spectral intensity distribution versus frequency, namely $\langle\nu\rangle = \sum_i \nu_i I(\nu_i) / \sum_i I(\nu_i)$ where the ν_i are the binned experimental Raman shifts, $I(\nu_i)$ is the associated intensity, and the sum is extended to the spectral range of the band (1550-1600 cm^{-1}). The comparison between $\Delta\nu$ and the SERS titration ratio r_{SERS} is displayed in **Figure S9**.

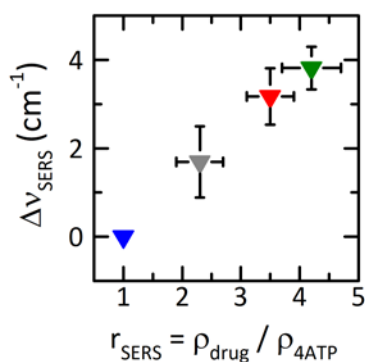


Figure S9: Comparison between the values of the CC-stretching band frequency shift $\Delta\nu$ and the SERS titration ratio r_{SERS} calculated as discussed above.

SI 5 - SEM on treated cells

In **Figure S10**, we report FESEM images acquired on tumorigenic (HeLa) and non-tumorigenic (HaCaT) cells treated with the AMT-NV at different concentrations. FESEM images were acquired at the CNIS Center for Nanotechnology and Innovation of Sapienza by employing an Auriga Zeiss electron microscope. The parameters employed are reported within the figures. The backscattering imaging mode was chosen for the imaging because it ensures a high contrast visibility of gold with respect to the biological sample, being the scattering cross section of gold higher than the one of the other materials present in the sample [Kri2005]. The samples are obtained by treating the cells as described in the Materials and Methods section of the main text, then rinsing the sample and drying them (the protocol is also described in [Fas2016]).

Some differences in the NV density on the membrane of HeLa/HaCaT cells is appreciable, reflecting the results presented in Figure 3 and 4 and related discussion in the main text.

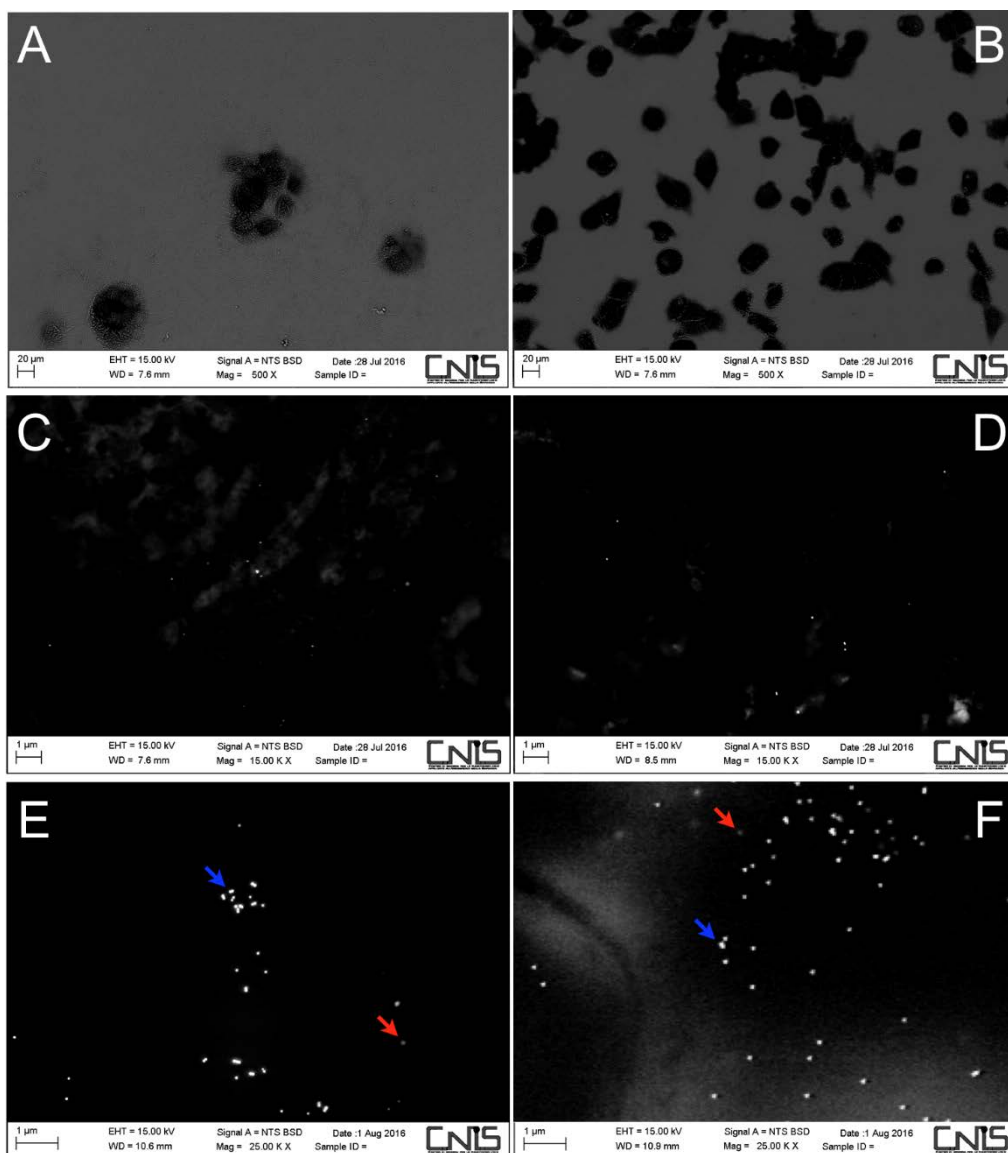


Figure S10: SEM imaging acquired in backscattering mode on HaCaT (left column) and HeLa cells (right column) cells, treated with the AMT-NVs for 24 hours at the concentrations of 1.25 pM (panels A, B, C, D) and 5 pM (panels E, F). A and B are field visions, allowing to distinguish the cells on the Si substrate. In panels E and F, the red arrows highlight NVs imaged with a different contrast, that is probably due to the NPs being covered by the cell membrane. The blue arrows instead indicate NVs that are anchored externally with respect to the membrane.

SI 6 - Effect of drug nanostructuring: case of MTX

In **Figure S11** we compare the effect of AMT and MTX on the viability of HeLa cells. These have been treated with the drugs in the NV form (columns on the left) and in the free molecular form (columns on the right) at selected concentrations. Even if the whole comparative study on the effect of drug nanostructuring (Figure 3 in the main text for the case of AMT) has not been performed in the case of MTX, the results in Figure S11 demonstrate that drug nanostructuring is convenient for both AMT and MTX. Indeed, comparable effects against cancer cells can be obtained employing a concentration of NV that is 4 orders of magnitude smaller than the one of free AMT. The absolute AMT concentration can be therefore decreased by a factor 10 when using the AMT-NV, as we load 1000 drug molecules per NP. These results demonstrate the general advantage of drug nanostructuring in this kind of systems.

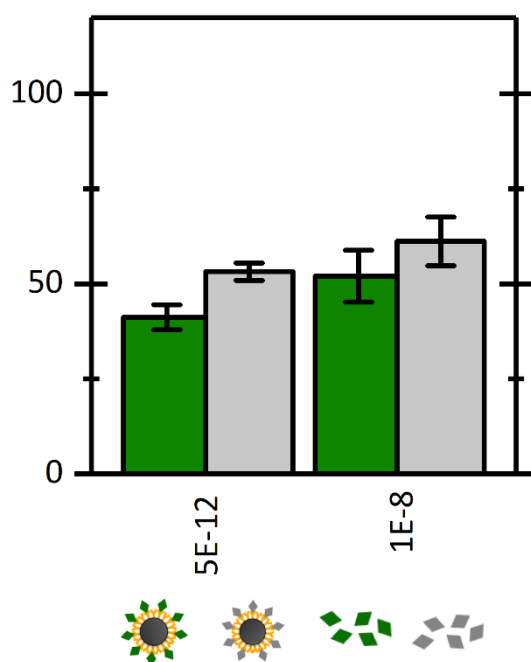


Figure S11: HeLa cell viability upon 24 hours treatment with AMT- and MTX-NVs, at 5 pM concentration (left columns, green: AMT, gray: MTX) and with AMT and MTX in the molecular form, at 10 nM concentration (right columns, green: AMT, gray: MTX).

REFERENCES

- [Fas2014]** Fasolato, C., Domenici, F., Sennato, S., Mura, F., De Angelis, L., Luongo, F., Costantini, F., Bordi, F. & Postorino, P. (2014). Dimensional scale effects on surface enhanced Raman scattering efficiency of self-assembled silver nanoparticle clusters. *Applied Physics Letters*, 105(7), 073105.
- [Kim2011]** Kim, N. H., Lee, S. J., & Moskovits, M. (2011). Reversible tuning of SERS hot spots with aptamers. *Advanced Materials*, 23(36), 4152-4156.
- [Osa1994]** Osawa, M., Matsuda, N., Yoshii, K., & Uchida, I. (1994). Charge transfer resonance Raman process in surface-enhanced Raman scattering from p-aminothiophenol adsorbed on silver: Herzberg-Teller contribution. *The Journal of Physical Chemistry*, 98(48), 12702-12707.
- [Zho2006]** Zhou, Q., Li, X., Fan, Q., Zhang, X., & Zheng, J. (2006). Charge Transfer between Metal Nanoparticles Interconnected with a Functionalized Molecule Probed by Surface-Enhanced Raman Spectroscopy. *Angewandte Chemie*, 118(24), 4074-4077.
- [Fas2018]** Fasolato, C. Investigation on Nanoparticles and Their Molecular Functionalization. In: *Surface Enhanced Raman Spectroscopy for Biophysical Applications*. Springer, Cham, 2018. p. 57-83.
- [Fas2016]** Fasolato, C., Giantulli, S., Silvestri, I., Mazzarda, F., Toumia, Y., Ripanti, F., Mura, F., Luongo, F., Costantini, F., Bordi, F., Postorino, P., and Domenici, F. (2016). Folate-based single cell screening using surface enhanced Raman microimaging. *Nanoscale*, 8(39), 17304-17313.
- [Kho2012]** Kho K. W., Dinish U. S., Kumar A., and Olivo, M. (2012). Frequency Shifts in SERS for Biosensing. *ACS Nano*, 6, 4892-4902.
- [Gue2013]** Guerrini, L., Pazos, E., Penas, C., Vázquez, M. E., Mascareñas, J. L., and Alvarez-Puebla, R. A. (2013). Highly sensitive SERS quantification of the oncogenic protein c-Jun in cellular extracts. *Journal of the American Chemical Society*, 135(28), 10314-10317.
- [Wan2014]** Wang, Y., Ji, W., Sui, H., Kitahama, Y., Ruan, W., Ozaki, Y., and Zhao, B. (2014). Exploring the Effect of Intermolecular H-Bonding: A Study on Charge-Transfer Contribution to Surface-Enhanced Raman Scattering of p-Mercaptobenzoic Acid. *The Journal of Physical Chemistry C*, 118(19), 10191-10197.
- [Tan2016]** Tang, B., Wang, J., Hutchison, J. A., Ma, L., Zhang, N., Guo, H., Hu, Z., Li, M., and Zhao, Y. (2016). Ultrasensitive, multiplex Raman frequency shift immunoassay of liver cancer biomarkers in physiological media. *ACS Nano*, 10(1), 871-879.
- [Zhu2018]** Zhu, W. F., Cheng, L. X., Li, M., Zuo, D., Zhang, N., Zhuang, H. J., Xie, D. Zeng, Q.D., Hutchison, J.A., and Zhao, Y. L. (2018). Frequency Shift Raman-Based Sensing of Serum MicroRNAs for Early Diagnosis and Discrimination of Primary Liver Cancers. *Analytical chemistry*, 90(17), 10144-10151.
- [Kri2005]** Krinsley, D. H. et al. "Backscattered scanning electron microscopy and image analysis of sediments and sedimentary rocks." Cambridge University Press, 2005.